10-2020

Effect of Lanthanum Doping on the reactivity of unsupported CoMoS2 catalysts

Carolina Valdes
The University of Texas Rio Grande Valley

Diego Gonzalez

Kenneth Flores
The University of Texas Rio Grande Valley

Thomas Eubanks
The University of Texas Rio Grande Valley

John Valle
The University of Texas Rio Grande Valley

See next page for additional authors

Recommended Citation

Valdes C, Gonzalez D, Flores K, Eubanks TM, Valle J, Hernandez C, Lopez J, Alcoutlabi M, Parsons JG, Effect of Lanthanum Doping on the reactivity of unsupported CoMoS2 catalysts, Applied Catalysis A, General (2020), doi: https://doi.org/10.1016/j.apcata.2020.117891

Effect of Lanthanum Doping on the reactivity of unsupported $CoMoS_2$ catalysts

Carolina Valdes[1], Diego Gonzalez[1], Kenneth Flores[1], T. M. Eubanks[1], John Valle[1], Carlos Hernandez[2], Jorge Lopez[2], Mataz Alcoutlabi[2], J.G. Parsons[1]* jason.parsons@utrgv.edu

[1]Department of Chemistry University of Texas Rio Grande Valley. 1 W University Blvd. Brownsville TX 78521

[2]Department of Mechanical Engineering University of Texas Rio Grande Valley. 1201 University Dr. Edinburg TX 78539

*Corresponding Author: Tel (956)882-7772

Graphical abstract

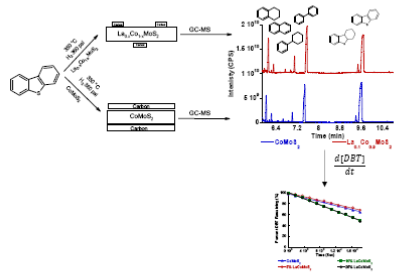

Highlights:

- A triphasic La-Co-Mo sulfide HDS catalyst was successfully synthesized using solvothermal synthesis
- $LaCoMoS_2$ showed enhanced activity over $CoMoS_2$ catalysts.
- The $LaCoMoS_2$ activity as improved with increasing La doping
- $LaCoMoS_2$ showed less carbon than $CoMoS_2$ after once catalytic cycle.
- The La doping of the $CMoS_2$ catalyst led to improvement in the direct desulfurization pathway.

Abstract:

In the present study, catalytic systems based on La-doping were developed to improve the activity and performance of $CoMoS_2$ hydrodesulfurization catalysts. Lanthanum-doped at 5, 10, or 25% of the Co content in $CoMoS_2$ hydrodesulfurization catalysts were synthesized through a solvothermal process. X-ray diffraction (XRD) and X-ray photoelectron spectroscopy (XPS)

analyses confirmed the catalysts were triphasic consisting of Co_9S_8, MoS_2, and La_2S_3. The La doped catalysts showed enhanced catalytic activity compared with $CoMoS_2$ synthesized under the same conditions. The $CoMoS_2$ prepared under solvothermal synthesis conditions showed a catalytic activity of 6.80 mol g^{-1} s^{-1}, however, the $La_{0.05}Co_{0.95}MoS_2$ doping showed a catalytic activity of 6.51 mol g^{-1} s^{-1} whereas the $La_{0.1}Co_{0.9}MoS_2$ and $La_{0.25}Co_{0.75}MoS_2$ samples showed catalytic activities of 10.7 mol g^{-1} s^{-1}. The reaction products indicated the major reaction pathway was direct desulfurization. The $La_{0.25}Co_{0.75}MoS_2$ catalyst after one reaction cycle showed a lower amount of carbon, than the undoped $CoMoS_2$ catalyst.

Keywords: La doping, hydrodesulfurization catalyst, $CoMoS_2$, triphasic, dibenzothiophene

Introduction:

Hydrodesulfurization (HDS) catalysis has been widely studied for the removal of sulfur from oil during production. Regulations from the EPA in 1993 reduced the allowable sulfur amount in fuels from 5000 ppm to 500 ppm, and later to 15 ppm in 2006, with implementations expected for ultra-low sulfur fuels to be 10 ppm on an annual average following 2017 [1]. The continuously high demand for ultra-low sulfur fuels has increased the need for the petrochemical industry to use high efficiency HDS catalysts. Traditional synthesis methods for HDS catalysts are environmentally unfavorable due to the production processes, which require high temperatures and the use of hydrogen sulfide (H_2S) gas. In addition, traditional HDS catalysts require high temperatures and pressures of hydrogen (H_2) to function efficiently. However, the current HDS catalyst research has shifted towards new synthesis techniques and the development of efficient HDS catalysts with more favorable operating conditions and cost effectiveness.

Currently, methods used for the synthesis of HDS catalysts consist of co-precipitation and incipient wet impregnation of silica or γ-alumina supports [2,3]. The synthesis of catalysts with

supports generally yield metal oxide precursors, which require thermal conversion under mixtures of H_2 and H_2S, yielding the active metal sulfide catalysts. To reduce the use of H_2 and H_2S during the catalyst synthesis, and to increase catalytic activities, the research focus has shifted towards unsupported catalysts with synthesis routes involving the use of alternative sulfide sources such as organic sulfide compounds, ammonium sulfide, and elemental sulfur [4,5,6]. New synthesis techniques have also included new methods for unsupported catalysts such as thermal decomposition of thiol salts, in situ decomposition of catalyst precursors in the reaction mixture and hydrothermal/solvothermal synthesis [7,8,9]. Recent research efforts on unsupported HDS catalysts have focused on the synthesis of MoS_2 and WS_2-based materials promoted with transitional metals such as cobalt (Co) or nickel (Ni). Alloying cobalt or nickel with these metal sulfides leads to a biphasic catalyst composed of Co_9S_8 or Ni_3S_4 and MoS_2 or WS_2 [9]. Novel synthesis methods of HDS catalysts are being investigated to eliminate the need for H_2S in the synthesis and reduce reaction temperatures. Sollner et al. used elemental sulfur for the synthesis of Co promoted MoS_2 [5] while Alonso et al. studied the synthesis of MoS_2 and WS_2 using alkyltrimethylammonium-thiomolybdate-thiotungstate-cobaltate (II) as the sulfur precursor [6]. Both elemental sulfur and alkyltrimethylammonium-thiomolybdate-thiotungstate-cobaltate (II) sulfur precursors have been shown to be successful sources for the synthesis of high efficiency HDS catalysts. The results showed that the catalytic activities were 32.7 x 10^{-6} mol l^{-1} s^{-1} g^{-1} and 13.6 x 10^{-6} mol l^{-1} s^{-1} g^{-1} for those synthesized with elemental sulfur and 5.1 x 10^{-6} mol l^{-1} s^{-1} g^{-1} and 4.6 x 10^{-6} mol l^{-1} s^{-1} g^{-1} for in situ decomposed catalysts synthesized with Ammonium tetrathiomolybdate (ATM) and ammonium thiotungstate (ATT), respectively [5,6].

Although the current research shows that the catalysts are highly active, the disadvantage is the poisoning of HDS catalysts through multiple processes such as sintering, metal segregation,

and the carbon buildup on the surface of the catalysts during use, all resulting in a gradual decrease in catalyst functionality [10-19]. The development of carbon on the surface of the catalysts, also known as coking of the catalysts, results in poisoning, which in turn leads to a reduction in efficiency, lifetime, and catalyst cyclability, which is especially evident in heavy feeds [10-19]. The solvothermal and in situ decompositions of HDS catalysts result in carbon buildup on the surface of the catalysts due the solvothermal reaction used to convert the precursor to the active catalysts [20]. For both Co and Ni based catalysts, carbon deposition is known to be a deactivating agent which can reduce the catalysts' efficiency and stability in different catalytic systems [21]. For example, research on Co and Ni based catalysts for Fischer-Tropsch synthesis and syngas production from biomass has been focused on minimizing catalytic poisoning. Numerous promoters have been studied for these catalysts including but not limited to, the use of lanthanum due to its ability to minimize carbon formation on the catalyst surface. Hemmati et al. analyzed the effects of lanthanum doping on γ-alumina supported Co and concluded that at optimal doping concentrations, the lanthanum enhanced the catalytic activity and prolonged catalyst lifetime [22]. However, there was no observable effect of lanthanum on the Co dispersion on the surface of the catalyst, leaving catalytic active sites unaffected. Similar results have been observed for Ni/γ-alumina and Ni/Al – following the addition of lanthanum, the catalytic efficiency and selectivity resulted in significant improvements in toluene reforming and syngas conversions [23-25]. Schacht et al. investigated the doping of TiO_2 supports of $CoMoS_2$ catalysts with La or Ce [26]. The authors observed a small increase in the catalytic activity in the presence of La at 2%, which showed increased activity to 70% versus 50% conversion observed with Ce doping. Therefore, it is important to develop new catalytic systems based on La-doping with improved activity, cost and performance, which is the focus of the present work. The main goal of the present work is to

develop new catalytic systems based on La-doping to improve the activity, cost and performance of $CoMoS_2$ hydrodesulfurization catalysts.

Unsupported Co promoted MoS_2 HDS catalysts were synthesized and doped with different concentrations of lanthanum to investigate the effects of La on the HDS reaction of dibenzothiophene (DBT). The catalyst precursors were prepared using a reflux reaction containing cobalt chloride, ATM and different concentrations of lanthanum nitrate in aqueous solutions. The precursors were converted into the $CoMoS_2$ catalysts using a solvothermal route with decahydronapthalene (decalin) as the solvent under hydrogen at 350 °C. The solvothermal synthesis technique was used in the present study to add carbon content to the surface of the catalysts with the aim to determine the effects of carbon deposition and lanthanum doping on the catalyst performance and activity. The structure and morphology of the $La_xCo_{1-x}MoS_2$ catalysts were characterized (or investigated), prior and after one catalytic cycle, using XRD, SEM/EDS, and XPS. The progress of HDS reaction was followed using GC-FID and GC-MS, to determine the reaction products, kinetics, and the catalytic activities of the La-doped $CoMoS_2$ HDS catalysts.

Experimental

Preparation of ATM

Ammonium tetrathiomolybdate was synthesized using a previously described method in that the ammonium sulfide was the sulfur source, [27]. A mass of 5.0 g of ammonium heptamolybdate was dissolved in 50 mL of 28% NH_4OH solution containing 60 mL of $(NH_4)_2S$. The solution was heated to 70°C under constant stirring and held at that temperature for 1 hr. The

product was cooled in an ice bath, filtered using vacuum filtration, and washed using isopropyl alcohol.

Preparation of HDS precursors

The catalyst precursors were prepared by dissolving 2.0 g of ATM and an equimolar amount of cobalt (II) chloride in 100 mL of deionized (DI) water (18MΩ resistance). The lanthanum doping of the samples was conducted by the addition of lanthanum (III) nitrate at 5%, 10% and 25% of the molar concentration of the cobalt (II) chloride to the precursor. The cobalt and lanthanum doped samples were heated under constant stirring to reflux at 100 °C for 2 hr. After heating, the samples were cooled to room temperature and filtered using vacuum filtration. The product was washed twice with water followed by acetone and air dried.

Solvothermal Synthesis of the HDS catalyst

One gram of the dried precursor and 100 mL of decalin solvent were placed in a 300 mL glass lined Parr model 4843 reactor and purged with H_2 gas three times, with a final pressure at160 psi at room temperature. The reaction vessel was heated to 350°C and the pressure of the reaction reached 360 psi and both, temperature and pressure were held constant during the reaction and a constant stirring rate of 150 RPM. The reactor was cooled to room temperature then the powder was collected by vacuum filtration and washed three times with acetone. The sample was air dried overnight before characterization and testing.

Catalytic testing of $La_xCo_{1-x}MoS_2$

The testing of the catalyst was performed using a previously determined HDS experimental method (or procedure). In brief, the test was performed using a solution containing 2.625 g DBT dissolved in 50 mL of decalin with 0.375 g catalyst using a 160 psi H_2 atmosphere, in a 300 mL glass lined Parr model 4843 reactor at 350 °C. Prior to each reaction, the reactor was purged three

times with H_2 gas. Once the reaction temperature was reached 350 °C, a 1.0 mL aliquot was extracted, subsequently at 30-minute intervals. The 1.0 mL aliquots were removed over a reaction time of 5 hr.

Catalyst Characterization:

XRD characterization

XRD characterization of the fresh and spent catalysts were performed using a Rigaku Miniflex II X-ray diffractometer. The working parameters of the XRD were as follows: 0.05° step in 2 θ, 5 s counting time, copper source operating at 30 kV and 15 mA (Kα 1.54 Å), nickel filter and scintillation detector. The extracted data were fitted using the Fullprof software while the LeBail fitting procedure and crystallographic data were obtained from literature [28-31].

Surface aera and Porosity

Structural properties of the $CoMoS_2$ and the La doped $CoMoS_2$ catalysts were determined by N_2 physisorption using a Quantachrome Instruments ANOVA 2200E Surface aera porosity instrument. The Samples were degassed under vacuum at 300°C for 3 h to removed adsorbed molecules. The surface area was determined using the Brunauer-Emett-Teller (BET,) method.

SEM/EDS characterization

The SEM characterization was conducted using a Zeiss EVO LS 10 electron microscope with an attached EDAX EDS detector. The data were collected using an operating voltage of 10.71-20.71 keV at a working distance between 6.0-6.5 mm. The EDS data were collected at an accelerating voltage of 20.71 keV with a 120 sec count time per sample.

XPS characterization

The XPS characterization was performed using a Thermo Scientific K-α XPS. The operating parameters were as follows: a micro-fused monochromatic Al K-α source with scans at

1 eV, a depth analysis at 1keV, and a 400 μm spot.

GC-MS/GC-FID characterization

The extracted sample aliquots from the catalytic testing cycle were analyzed using GC-MS and GC-FID for the conversion of DBT. The GC-MS was used to identify the potential products while the GC-FID was used to monitor the reaction after identification of the final product. The extracted reaction aliquots were tested using a Perkin Elmer Autosystem XL attached to Turbomass Gold mass spectrometer and a Perkin Elmer Clarus GC with a flame ionization detector. The GC-MS and GC-FID operating conditions are summarized in Table 1.

Results and Discussion

XRD characterization

Figure 1 shows the diffraction pattern for the as-synthesized ATM precursor resulting in an orthorhombic crystal lattice, with LeBail fittings illustrated in Table 2. The synthesized ATM precursor crystallographic parameters were in good agreement with that reported on the same material, with an overall χ^2 value reduced to 2.54, indicating a small difference between the data and fitting [32].

The diffraction patterns for the catalysts synthesized under a solvothermal decomposition are shown in Figure 2 while the assoicated LeBail fittings are shown in Table 3. MoS_2 had a hexagonal phase with stacking occuring on the 002 plane corresponding to the peak at 14° in 2θ, the relatively low intensity and broadness of this peak indicated low stacking of the MoS_2 planes [33]. A low stacking of MoS_2 planes is commonly observed for $CoMoS_2$ HDS catalysts [34]. The shoulder peak at 15.44° in 2θ corresponds to the (111) plane of Co_9S_8 [35]. Furthermore, the synthesis of $CoMoS_2$ is dictated by the formation of MoS_2 phase because it forms at a higher temperature than that for Co_9S_8. The formation and crystallinity of these HDS catalysts are highly

dependent on the synthesis conditions. When using ATM as a precursosr, Yoosuk et al. observed that the formation of Co and Ni promoted MoS_2 started at lower temperatures of 383 °C and 366 °C, respectively[9]. Similarly, Ramos et al. reported that when using ATM as a catalyst precursor, the formation of MoS_2 began at 350 °C [36]. Comparable to these findings, Alonso et al., reported the formation of $NiWS_2$ *in situ* during the HDS of DBT at 350 °C when using ATT precursor [37].

Catalysts with lanthanum dopings at 5 and 10 % weight resulted in no observable changes in the diffraction patterns, only two identifiable phases of Co_9S_8 and MoS_2 were obsrved. However, a La-doping concentration of 25 % introduced a third phase, La_2S_3 was observed in the diffraction pattern of $La_{0.25}Co_{0.75}MoS_2$, (Figure 2). The new peaks were attributed to the formation of La_2S_3, located at 12.6°, 19.4° and 25.7° in 2θ, which corresponds to (101), (103), and (202) planes, respectively. When considering the orthorombic La_2S_3 phase, there is an excellent agreement between the data and that reporetd in the literature [38]. Table 3 summarizes the LeBail fitting results for solvothermally synthesized La doped and undoped $CoMoS_2$ catalysts, with reduced χ^2 values and their corresponding fittings ranging from 0.170 and 0.379. The addition of the La doping to the $CoMoS_2$, in the diffraction pattern did not have a large effect on the MoS_2 crystallintiy. However, the additon of the La had an apparent effect of increasing the cryatlling of the Co9S8 phase, as indicated by the decreasing full width half maximum (FWHM) of the diffraction peaks located at 29.8, 47.5 and 52.1. The diffraction peakes located in the CoMoS2 at 29.8, 47.5 and 52.1 (2□) decreased from 0. 43, 1.07 1.07 to: 0.26, 0.37,0.37 in the $La_{0.05}Co_{0.95}MoS_2$, 0.28, 0.43, and 0.39 for the $La_{0.10}Co_{0.90}MoS_2$, and to 0.036, 043, and 0.45 for the $La_{0.25}Co_{0.75}MoS_2$ samples. With the La doping, the crystallinity of the Co9S8 phase in the samples increased with increasing La concentration.

The diffraction patterns of used catalyts are presented in Figure 3 with the associated LeBail fittings shown in Table 4. Following one catalytic cycle, the catalysts maintained their Co_9S_8 and MoS_2 crystal phases and La_2S_3 phase for the $La_{0.25}Co_{0.75}MoS_2$ catalyst. The χ^2 values of the fittings were between 0.183 and 0.469, indicating a minimal difference between each sample and their fittings. There were no observable changes in the FWHM of the Co_9S_8 phase after one reaction cycle. The conserved crystallinity of these catalysts indicated the presence of some stability in the crystallographic phases which can enhance the catalyst lifetime.

Surface aera Porosity analysis:

The N2 adsorption data used to determine the Surface area of the samples are shown in Table 5 The adsorption isotherms were observed to follow type II adsorption isotherm. The adsorption isotherm indicates the development of multiple layers of adsorbent on the surface during the adsorption process. The $CoMoS_2$, $La_{0.10}Co_{0.90}MoS_2$ and $La_{0.25}Co_{0.75}MoS_2$ samples show similar surface aeras with respect to total surface area ranging from 50-67 m2/g. However, the $La_{0.05}Co_{0.95}MoS_2$ doped sample shows a larger surface area as well as almost double of the surface area of the other La doped catalyst (with almost double the pore volume). The $La_{0.05}Co_{0.95}MoS_2$ does support the idea that La at low concertation inhibits the formation of the planes in MoS_2, which would result in higher surface area [39]. Furthermore, the increasing in the amount of La doping in the catalysts showed a decrease in the surface aera. Overall, the surface aera obtained in form the samples, is relatively low which his less than 100 m2/g.

SEM/EDS characterization results

The SEM images of the solvothermally decomposed catalysts are shown in Figure 4, which reveal the formation of platelets with small spherical particles clustered on the surface. Y. Wu has

reported the presence of spherical particles on the surface of $CoMoS_2$ catalysts synthesized from an ATM precursor with the addition of amines [40]. In the present study, the spherical particles, with an average size of 50 nm at 25% lanthanum doping. The $La_{0.05}Co_{0.95}MoS_2$ exhibited an agglomeration of particles with no definite morphology. The lack of morphological uniformity may be caused by the presence of cavities or defects formed during the synthesis of Co_9S_8 at elevated temperatures [41]. In addition, the presence of carbon on the sample surface may inhibited the imaging of the sample. Alternatively, it has been suggested that La doping at low concentration can inhibit the MoS_2 plane development [39].

Table 6 shows the Mo, S Co and La data collected using EDS analysis for the catalytic samples as synthesized and recovered after one catalytic cycle. The data indicate a loss of La from the $La_{0.05}Co_{0.95}MoS_2$ sample after one catalytic cycle, which would help to explain the slightly lower activity of the $La_{0.05}Co_{0.95}MoS_2$ compared to the other samples La-doped samples. There could be a stability issue within the samples at lower La concentrations, due to surface stain observed in some nanoparticles [ref]. Alternatively, the La in the before on catalytic cycle may not have been as tightly bound to the surface of the precursor and may have been lost during the catalytic cycle. On the other hand, the $La_{0.10}Co_{0.90}MoS_2$ and $La_{0.25}Co_{0.75}MoS_2$ remained relatively constant with respect to the amount of La present. In both, the $La_{0.10}Co_{0.90}MoS_2$ and $La_{0.25}Co_{0.75}MoS_2$ samples, the La concentration was approximately 50% of the intended ratio. These results do explain the absence of La_2S_3 diffraction in the $La_{0.10}Co_{0.90}MoS_2$ while the concentration of La_2S_3 was too low for diffraction. In addition, the lower concentrations also the diffuse XPS plots. The elemental distribution of molybdenum, sulfur, cobalt, lanthanum, and carbon for fresh $CoMoS_2$ and $La_{0.25}Co_{0.75}MoS_2$ catalysts are presented in the EDS images of Figures 5 (A and B), respectively.

It was observed that molybdenum and sulfur are closely associated in their distribution, while cobalt is distributed evenly throughout the surface. With the incorporation of lanthanum doping, the cobalt was displaced with lanthanum appearing in the cobalt vacancies. Under solvothermal decompositions, the use of organic solvents resulted in the presence of carbon on the surface of the catalysts and for this reason, the EDS mapping included the analysis of carbon [20]. It was observed that the concentration of carbon on the surface of the catalysts was significantly less than that observed for the other elements as shown by the low intensity in the EDS mapping of carbon element (Figures 5 and 6).

Figures 6 (A and B) include the EDS mappings of used $CoMoS_2$ and $La_{0.25}Co_{0.75}MoS_2$ catalysts, respectively. Similar results in the molybdenum, sulfur, cobalt and lanthanum distribution on the surface of the catalysts were observed following one catalytic cycle, with differences occurring with the carbon distribution on the samples. While, $CoMoS_2$ had an increase in carbon concentration on the surface of the catalysts, indicated by the higher intensity in the elemental mapping of carbon, the carbon in $La_{0.25}Co_{0.75}MoS_2$ appeared to decrease and disperse in the catalyst surface. Catalyst coking is an important issue that can minimize the efficiency and lifetime of catalysts [10]. It is believed that lanthanum doping contributed to the decrease of carbon on the surface of the $La_{0.25}Co_{0.75}MoS_2$ catalyst, as has been previously reported with lanthanum promoted catalysts [22-25, 42].

XPS results

The elemental composition and binding energies of the catalyst were evaluated by XPS. Figures 7A and 7B show the XPS results corresponding to the XPS survey spectra of fresh and used catalysts, respectively. Binding energies of 778.9 eV, 285.4 eV, 229.0 eV, and 161.9 eV,

were attributed to Co $2P_{3/2}$, C 1S, Mo $3d_{5/2}$, and S 2P, correspondingly, which is in a good agreement with results reported on unsupported $CoMoS_2$ catalysts [43].

Figure 8 (A-H) shows the Co2P XPS spectra collected for the synthesized samples, which includes the Co^{2+} $2P_{2/3}$ and Co^{2+} $2P_{1/2}$ peaks located at 778 eV and 794 eV, respectively [44- 46]. The broad peaks observed in the spectrum located at 782.5 eV and 799.9 eV are the Co $2P_{3/2}$ and Co $2P_{1/2}$ satellite peaks [44-46]. There may be some Co^{3+} spectrum mixed into the satellite peaks, which is located around 780.6 eV; however, it would be very minor to add additional fitting curves to the data to improve the fitting results [47]. In fact, additional fitting curves to the XPS data did not improve the fitting of the XPS spectrum. The XPS data suggests the presence of the cobalt as Co^{2+}, which is found in the Co_9S_8 phase of cobalt sulfide, which has been already observed at 778.2 eV and 793.2 eV for the Co $2P_{3/2}$ and Co $2P_{1/2}$ levels of Co_9S_8 species [48]. However, the presence of the CoMoS phase could not be determined in the XPS results of the present study. Typically, the CoMoS phase has an energy of 779.2-779.6 eV, which was not observed in the spectra of the samples (Figure 11) [49]. Another study showed that the CoMoS phase can be observed at 778.8 eV and 793.9 eV for the Co $2P_{3/2}$ and Co $2P_{1/2}$ peaks, respectively [48]. Also, at 778.6 and 778.1eV for the CoMoS and Co_9S_8 phases for the Co $2P_{3/2}$ peak, respectively [48]. A quick survey of the data in the literature shows a variation of approximately ± 1 eV on the position of the CoMoS phase. The error on the position of the CoMoS phase places it within the range of the Co_9S_8, Co_3S_4 (778.6 eV and 779.7 eV for the Co^{2+} and Co^{3+} ions, respectively), and CoS_2 (778.9 eV and 778.5 eV) energies [50, 51]. In addition, XPS results reported in the literature generally show a higher intensity and higher area of the spectra for the CoMoS phase than that for the Co_9S_8 phase, which would indicate a higher concentration of the CoMoS phase than for the actual major Co_9S_8 phase. The presence of the Co_9S_8 phase in the samples was determined using

XRD analysis (Figure 2). As can be seen in Figure 8 (A-H), the XPS survey spectra, before and after reaction, do not change dramatically, indicating that the Co phase is stable after synthesis and is still present after one reaction cycle. The Co 2P spectra were not shifted to higher/lower energy levels, indicating no reduction and no oxidation occurred in the cobalt.

Figure 9 (A-H) shows the S 2p region consisted of two main peaks located at binding energies of 161.9 eV and 163.1 eV, which correspond to S $2P_{3/2}$ and S $2P_{1/2}$, respectively [52]. The single doublet with the $2P_{3/2}$ peak located at 161.9 eV indicates that sulfur is present in the 2- oxidation state [52]. These S 2P peaks are associated with the presence of the metal sulfide phases, which include the MoS_2, Co_9S_8 and La_2S_3 phases present in the samples. There is a small shoulder peak located at 163.5eV corresponding to the presence of C-S bonds, which would be present after the solvothermal process. The conversion of all the catalysts was performed at 350 °C in decalin to generate the metal sulfide, which may have generated the carbon-sulfide bonds in the sample. The presence of carbon in the samples was also observed in the collected EDS data for both the as synthesized and the catalyst used in one reaction cycle, as was shown in Figures 5 and 6, respectively. In addition, a small amount of the sulfur present in the sample was oxidized as indicate by the S-O bond located at 169 eV, this was less than 10% of the sulfur present in the sample.

The Mo 3d survey spectra, (Figure 10 (A-H)), show two peaks being located at a binding energy (BE) of 229.7 eV and 232.3 eV, which can be assigned to the Mo $3d_{5/2}$ and Mo $3d_{3/2}$ core level transitions, respectively. The position of the peaks indicates the presence of Mo in the 4+ oxidation state and is present as MoS_2 [52, 53]. In addition, a third peak located at 226.5 eV is observed in all the spectra, which is assigned to the S 2S core level transition. In all the samples, before and after use, an additional peak is observed around the Mo $3d_{3/2}$ peak at approximately

232.5 eV in the $CoMoS_2$, before reaction, after reaction, and in the $La_{0.05}Co_{0.95}MoS_2$ sample before reaction. The 232.5 eV peak has been observed in the synthesis of molybdenum carbide samples and has been attributed to the formation of Mo-C bond in α-MoC_{1-x} phases [54]. The $CoMoS_2$ catalyst without La present, shows a large increase in the peak at 232.5 eV after one catalytic cycle, which would be expected if this were the formation of a Mo-C compound. It is also observed that the peak at 232.5 eV in the $La_{0.05}Co_{0.95}MoS_2$ catalysts is no longer present after the reaction, indicating that the sample is similar to the other La doped catalysts. Furthermore, a peak at 233.4 eV was observed for all the other samples. In the La-Co-MoS_2 samples, the feature at 233.4eV is well defined and does not change in magnitude after reaction, this peak has been assigned to the presence of Mo in the 6+ oxidation state which corresponds to the presence of a small amount of oxygen present in the samples. The presence of Mo-C in the samples after synthesis and after an increase in reaction cycles, would give an indication that the generation of the Mo-C phases occurs at the surface of the $CoMoS_2$ catalysts. However, the addition of the La to the sample prevents the formation of the Mo-C or reduces the concentration of the Mo-C. Similar results were observed on the EDS mappings of the catalysts in that the sample with La after one catalytic cycle showed less carbon on the catalyst surface compared to the catalysts without La. Furthermore, the addition of the La to the samples prevented the formation of the Mo-C phase, which may be poisonous to the catalysts, with reduced activity over time. Results reported in the literature showed that the addition of La to different catalysts prevented both, carbon build up and the generation of metal carbides [22-26, 42, 55, 56].

The La $3d_{5/2}$ spectra are shown in Figure 11 (A-F), which consist of two electronic transitions, the first is located at approximately 838.6 eV and the second at 834.5 eV. These two peaks observed in the La $3d_{5/2}$ spectrum can be attributed to binding lanthanum to sulfur in La_2S_3

and to the satellite peak for La [57]. The satellite peak is originated from the transition of a 3d electron into an empty 4f orbital, this transition is observed when La^{3+} is present in the sample [57-60] such as in La_2S_3. Similar XPS spectra are observed in Figure 11 (A, B, and C) for the as synthesized samples which indicate that La is in the same chemical environment in all the samples, before and after one catalytic cycle. However, La doping in catalysts has been investigated to reduce carbon buildup on the surface of the catalyst [22-26, 42, 56]. The presence of carbon on the surface of each catalyst was also analyzed in the XPS spectra due to the presence of decahydronaphthalene solvent during decomposition and HDS reactions. The relative changes in concentration of carbon on the surface of each catalyst were quantified by integrating the distinctive C 1s peak at 284.1 eV [61]. The ratio between integrated C 1s peaks of used to fresh catalysts are summarized in Table 6. It was determined that $CoMoS_2$ had the highest increase in carbon on the surface of the catalyst followed by $La_{0.05}Co_{0.95}MoS_2$. With the $La_{0.10}Co_{0.90}MoS_2$ catalyst, the presence of carbon remained the same, however, in the $La_{0.25}Co_{0.75}MoS_2$ the overall carbon content on the surface was reduced by 2.9%. These findings are in agreement with the observed EDS results in that the carbon mapping intensity decreased for $La_{0.25}Co_{0.75}MoS_2$ following one catalytic cycle compared to $CoMoS_2$ where an increase of carbon was observed.

Catalytic Performance of dibenzothiophene hydrodesulfurization:

The results for catalytic removal of DBT at 350℃ are shown in Figure 12. All the reaction kinetics followed a pseudo zero order kinetics model and were fitted accordingly. It was observed that La doping had similar effects on DBT conversion. For the $La_{0.10}Co_{0.90}MoS_2$ and $La_{0.25}Co_{0.75}MoS_2$, the catalytic activities were enhanced, showing a maximum of 42% DBT removal. Higher doping of La was not evaluated because that would greatly reduce Co_9S_8, which

is a well-known promoter of MoS_2 HDS catalysts [62]. In addition, there was no observed increase in the catalytic activity between $La_{0.10}Co_{0.90}MoS_2$ and $La_{0.25}Co_{0.75}MoS_2$ catalysts.

Catalytic activities were determined using rate constants from the kinetics data and calculated by an equation described by Alonso et al, shown below:

$$k_{cat} = \frac{k_{rxn}}{m_{cat}} \times 10^7$$

Where k_{cat} is the catalytic constant corrected for volume with units of mol $g^{-1}s^{-1}$, k_{rxn} is the rate constant corrected for volume with units of mol s^{-1}, m_{cat} is the mass of the catalyst, and 10^7 is a normalization constant [20]. Under the solvothermal decomposition, 10 % and 25 % La doped samples had the highest catalytic activity, of 10.7 mol g^{-1} s^{-1}. The 5 % La doping of the $CoMoS_2$ showed a small decrease increase in the catalytic rate to 6.51 mol g^{-1} s^{-1} from 6.80 mol g^{-1} s^{-1} for the $CoMoS_2$ catalysts. Escobar et al found La- doping of P-CoMo on alumina showed a decrease in the catalytic HDS process at from as La concentration was increased from 1% to 5%. However, the selectivity of the reaction towards biphenyl as the product was increased [63]. Our results show the lowest catalytic activity for the $La_{0.05}Co_{0.95}MoS_2$ sample and the catalytic active increased for both the $La_{0.10}Co_{0.90}MoS_2$ and $La_{0.25}Co_{0.75}MoS_2$. Similar catalysts have been studied, reporting pseudo-zero order kinetics with comparable catalytic activities of DBT conversion over a reaction period of 5 h. Sollner et al. used elemental sulfur for the synthesis of $CoMoS_2$, under high-temperature conditions, which showed two reaction rates of 24.5 and 9.27 mol s^{-1} g^{-1} [5]. Olivas et al investigated a Ni promoted MoS_2 catalyst under a H_2S/H_2 gas sulfidation and found the catalytic activity to be 7.2 mol g^{-1} s^{-1} [64]. Quintana-Melgoza et al has reported catalytic activities of 4.61 and 2.74 mol g^{-1} s^{-1} for $NiMoS_2$ and MoS_2, respectively, both synthesized under a H_2S/H_2 gas mixture [65]. Furthermore, for the current used catalyst in industry, $NiMoS_2$ has been reported to have a catalytic activity in the range of 11 mol g^{-1} s^{-1}[66]. Table 8 shows the catalytic

activities of HDS catalysts reported in literature which are comparable to the values determined for the catalysts in the present work. The data presented in this work suggest that lanthanum doping at optimal concentrations may enhance catalytic activity and effectively enhance catalytic lifetime observed through the reduction of catalyst coking. In addition, a solvothermal decomposition was performed using $(NH_4)_2S$ as the sulfur source, which eliminated the need of conventional sulfidation processes such as H_2S/H_2 flow [66]. Furthermore, many of the reported catalysts require thermal decompositions at 450 ℃ or greater; however, in the present study, $CoMoS_2$ was successfully synthesized at 350 ℃.

Products from the HDS reactions were identified and analyzed from the data obtained from GC-MS and GC-FID. The overall reaction products observed were biphenyl, tetrahydrodibenzothiophene, and cyclohexylbenzene, as was determined using GC-MS. Moreover, biphenyl was the major product observed for the reaction followed by cyclohexylbenzene and tetrahydrodibenzothiophene. The presence of biphenyl and tetrahydrodibenzothiophene elucidate the presence of two competing reaction processes, direct desulfurization (DDS) and indirect desulfurization (HYD). Figure 13 shows the chromatograms for the $CoMoS_2$ and the $La_{0.1}Co_{0.9}MoS_2$ when the reaction has reached temperature. There is a small amount of biphenyl present the reaction starts slightly before reaching 350°C as well as a solvent peak from tetrahydronaphthalene. Figure 14 shows the reaction products after 300 minutes of reaction time which shows the presence of unreacted DBT, hydrogenated DBT, Biphenyl, cyclohexylbenzene. As well naphthalene and tetrahydronaphthalene are observed, which are dehydrogenation products of the decahydronaphthalene. The relatively high amount of biphenyl indicates that DDS is the primary pathway for the catalysts in this study as is common for Co

promoted MoS_2 catalysts reported in literature also supports the promotion of the catalyst into the DDS pathway caused by La doping observed in the literature [68, 63].

Conclusions:

A lanthanum doped $CoMoS_2$ HDS catalyst was successfully synthesized through a $(NH_4)_2MoS_4$ precursor, cobalt (II) chloride, and lanthanum nitrate using solvothermal conversion. The catalyst exhibited enhanced activity when compared to $CoMoS_2$ synthesized under the same reaction and conversion conditions. The 10 and 25 % La doped samples showed almost double the reactivity of the non-doped $CoMoS_2$ catalyst. The catalysts were determined to be triphasic consisting of a Co_9S_8, MoS_2 and La_2S_3. The La-doped catalysts showed the presence of La_2S_3 phase according to the X-ray diffraction and XPS data analysis of the catalyst with the highest La concentration. In addition, EDS mapping and XPS data indicated that carbon build up was reduced in the presence of higher concentrations of La (10 and 25 % doping) in the sample. The data also showed that the direct desulfurization was the preferred reaction pathway for both the $CoMoS_2$ and $La_xCo_{1-x}MoS_2$ catalysts with biphenyl as the major reaction product.

Credit Author Statement

Carolina Valdes: was responsible for data collection, synthesis of the materials, experimentation, and analysis and writing the first draft
Diego Gonzalez: was responsible for data collection and experimentation and helping with the first draft of the manuscript
K. Flores: was responsible for data collection and experimentation and helping with the first draft of the manuscript
John Valle: was responsible for helping with experimentation and data collection
T. M. Eubanks: was responsible for SEM data collection and interpretation
J. Lopez and C. Hernandez were responsible for the collection of the XPS data
M. Alcoutlabi was responsible for helping with writing and editing the manuscript as well as the XPS data collection.
J.G. Parsons is the corresponding author, project administrator was responsible for: the conceptualization of the project , for finalizing the manuscript and final draft writing of the manuscript. AS well as over seeing the data analysis and interpretation.

Declaration of interests

The authors declare that they have no known competing financial interests or personal relationships that could have appeared to influence the work reported in this paper.

Acknowledgements:

The Department of Chemistry at the University of Texas Rio Grande Valley is grateful for the generous support provided by a Departmental Grant from the Robert A. Welch Foundation (Grant No. BX-0048). M. Alcoutlabi acknowledges support from NSF PREM (DMR-1523577): UTRGV-UMN Partnership for Fostering Innovation by Bridging Excellence in Research and Student Success.

References:

[1] EPA (2011) Diesel Fuel Standards and Rulemakings. US Environmental Protection Agency https://www.epa.gov/diesel-fuel-standards/diesel-fuel-standards-and-rulemakings

[2] H. Topsoe, N.-Y. Topsoe, O. Sorensen, R. Candia, B.S. Clausen, S. Kallesoe, E. Pedersen, R. Nevald (1985) The role of promoter atoms in cobalt-molybdenum and nickel-molybdenum catalysts. Solid State Chemistry in Catalysis 14:235-246.

[3] C-L. Chen, S.-S. Lin, and T.-C. Liu (2002) Effect of catalyst preparation conditions on the hydrodesulfurization of thiophene over Co-Mo/γ-Al2O3. Journal of Environmental Science and Health, Part A 6:1147-1157.

[4] Y. Espinoza-Armenta, J. Cruz-Reyes, F. Paraguay-Delgado, M. Del Valle, G.Alonso, S. Fuentes, R. Romero-Rivera (2014) CoMoW sulfide nanocatalysts for the HDS of DBT from novel ammonium and alkyltrimethylammonium-thiomolybdate-thiotungstate-cobaltate (II) precursors. Applied Catalysis A: General 486:62-68.

[5] J. Sollner, D.F. Gonzalez, J.H. Leal, T.M. Eubanks. J.G.Parsons (2017) HDS of dibenzothiophene with CoMoS2 synthesized using elemental sulfur. Inorganica Chimica Acta 466:212-218.

[6] G. Alonso, M. Del Valle, J. Cruz, A. Licea-Claverie, V. Petranovskii, S. Fuentes (1998) Preparation of MoS2 and WS2 catalysts by in situ decomposition of ammonium thiosalts. Catalysis Letters 52:55-61.

[7] H. Nava, F. Pedraza, G. Alonso (2005) Nickel-Molybdenum-Tungsten Sulphide catalysts prepared by in situ activation of tri-metallic (Ni-Mo-W) alkylthiomolybdotunstates. Catalysis Letters 99:65-71.

[8] J. Cruz-Reyes, M. Avalos-Borja, M.H. Farias, S. Fuentes (1991) Mixed impregnated thiosalt decomposition catalysts characterized by x-ray diffraction. Catalysis Letters 9:387-394.

[9] B. Yoosuk, J. Hyung Kim, C. Song, C. Ngamcharussrivichai, P. Prasassarakich (2008) Highly active MoS2, CoMoS2 and NiMoS2 unsupported catalysts prepared by hydrothermal synthesis for hydrodesulfurization of 4,6-dimethyldibenzothiophene. Catalysis Today 130:14-23.

[10] E.E. Wolf, and F. Alfani (1983) Catalysts Deactivation by Coking. Catalysis Reviews-Science and Engineering 24:329-371.

[11] G. Alonso, V. Petranovskii, M. Del Valle, J. Cruz-Reyes, A. Licea-Claverie, S. Fuentes (2000) Preparation of WS2 catalysts by in situ decomposition of tetraalkylammonium thiotungstates. Applied Catalysis A: General 197:87-97.

[12] S. Song, S. Ihm. (2003) Deactivation control through accelerated precoking for the CoMo/γAl2O3 catalysts in thiophene hydrodesulfurization. Korean J. Chem. Eng. 20: 284–287.

[13] Bas M. Vogelaar, Petr Steiner, A. Dick van Langeveld, Sonja Eijsbouts, Jacob A. Moulijn. (2003) Deactivation of Mo/Al2O3 and NiMo/Al2O3 catalysts during hydrodesulfurization of thiophene. Applied Catalysis A: General. 251: 85-92.

[14] Bertrand Guichard, Magalie Roy-Auberger, Elodie Devers, Christophe Pichon, Christelle Legens Philippe Lecour. (2010) Influence of the promoter's nature (nickel or cobalt) on the active phases 'Ni(Co)MoS' modifications during deactivation in HDS of diesel fuel. Catalysis Today. 149: 2-10.

[15] Jae HyunKoh, Jung Joon Lee, Heeyeon Kim, Ara Cho, Sang Heup Moon. (2009) Correlation of the deactivation of CoMo/Al2O3 in hydrodesulfurization with surface carbon species. Applied Catalysis B: Environmental. 86: 176-181.

[16] R. Nava, A. Infantes-Molina, P.Castaño, R. Guil-López, B. Pawele. (2011) Inhibition of CoMo/HMS catalyst deactivation in the HDS of 4,6-DMDBT by support modification with phosphate. Fuel. 90: 2726-2737.

[17] Jorge Noé Díaz de León, Chowdari Ramesh Kumar, Joel Antúnez-García, Sergio Fuentes-Moyado. (2009) Recent Insights in Transition Metal Sulfide Hydrodesulfurization Catalysts for the Production of Ultra Low Sulfur Diesel: A Short Review. Catalysts. 9: 87.

[18] P. Dufresne. (2007) Hydroprocessing catalysts regeneration and recycling. Appllied Catalysis A: General. 322: 67–75.

[19] Morteza Baghalha, Seyed Mohammad Hoseini. (2009) Long-Term Deactivation of a Commercial CoMo/γ-Al2O3 Catalyst in Hydrodesulfurization of a Naphtha Stream. Industrial and Engineering Chemical Research. 48: 3331–3340

[20] S.K.Maity, E.Blanco, J. Ancheyta, F.Alonso, H.Fukuyama (2012)Early stage deactivation of heavy crude oil hydroprocessing catalysts. Fuel. 100: 17-23.

[21] Hale Ay, Deniz Uner (2015) Dry reforming of methane over CeO2 supported Ni, Co and Ni-Co catalyst. Applied Catalysis B: Environmental 179:128-138.

[22] M. Reza Hemmati, M. Kazemeini, J. Zarkesh, F. Khoresheh (2012) Effect of lanthanum doping on the lifetime of Co/ γ-Al2O3 catalysts in Fischer-Tropsch synthesis. Journal of the Taiwan Institute of Chemical Engineers 43:704-710.

[23] S. Bona, P. Guillen, J. German Alcalde, L. Garcia, R. Bilbao (2008) Toluene steam reforming using coprecipitated Ni/Al catalysts modified with lanthanum or cobalt. Chemical Engineering Journal 137:587-597.

[24] S. Wang, GQ Lu (2000) Effects of promoters on catalytic activity and carbon deposition of Ni/γ-Al2O3 catalysts in CO2 reforming of CH4. Journal of Chemical Technology and Biotechnology 75:589-595.

[25] S.A. Hanafi, H. A. El-Syed, M. S. Elmelawy and E.-S. A. Sultan (2009) Study of the Role of Lanthanum Containing Titania in Hydrogenolysis of Thiophene and Gas Oil. Energy Sources, Part A 31:831-842.

[26] P. Schacht, G. Hernandez, L. Cedeno, J. H. Mendoza, S. Ramirez, L. Garcia, J. Ancheyta. (2003) Hydrodesulfurization Activity of CoMo Catalysts Supported on Stabilized TiO2. Energy Fuels. 17: 81–86.

[27] Yan-Hua Dai, Ling-Bin Kong, Kun Yan, Ming Shi, Tong Zhang, Yong-Chun Luo, Long Kang (2016) Simple synthesis of a CoMoS4 based nanostructure and its application for high performance supercapacitors. RSC Advances 6:7633-7642.

[28] J. Rodriguez-Carvajal (1993) Recent advances in magnetic structure determination by neutron powder diffraction. Physica B 192:55-69.

[29] A Le Bail, H Duroy, J L. Fourquet (1988) Ab-initio structure determination of LiSbWO6 by X-ray powder diffraction. Mater. Res. Bull. 23:447-452.

[30] S. Geller (1962) Refinement of the crystal structure of Co9S8. Acta Cryst.15:1195-1198.

[31] R.G. Dickinson, L. Pauling (1923) The Crystal Structure of Molybdenite. J. Am. Chem. Soc., 45:1466-1471.

[32] Bjorn Hill, Hans-Wolfram Lerner, Michael Bolte (2010) Redetermination of diammonium thiomolybdate Acta Crystallographica Section E 66: i13. https://doi.org/10.1107/S1600536810003016.

[33] R.R. Chianelli, E.B. Prestridge, T.A. Pecoraro, J.P. Deneufville (1979) Molybdenum Disulfide in the Poorly Crystalline "Rag" Structure. Science 203:1105-1107.

[34] M. Del Valle, J. Cruz-Reyes, M. Avalos-Borja, S. Fuentes (1998) Hydrodesulfurization activity of MoS2 catalysts modified by chemical exfoliation. Catalysis Letters 54:59-63.

[35] Peng-Fei Yin, Li-Li Sun, You-Lu Gao, Sheng-Yue Wang (2008) Preparation and characterization of Co9S8 nanocrystalline and nanorods. Bulletin of Materials Science 31:593-596.

[36] M. Ramos, G. Berhault, D.A. Ferrer, B. Torres, and R.R. Chianelli (2012) HRTEM and molecular modeling of the MoS2-Co9S8 inerface: understanding the promotion effect in bulk HDS catalysts. Catalysis Science and Technology 2:164-178.

[37] G. Alonso, J. Espino, G. Berhault, L. Alvarez, J. L. Rico (2004) Activation of tetraalkylammonium thiotungstates for the preparation of Ni-promoted WS2catalysts.Applied Catalysis A: General : 266:29-40.

[38] F. H. Spedding, A. H. Daane and K. W. Herrmann (1956) The Crystal Structures and Lattice Parameters of High-Purity Scandium, Yttrium and the Rare Earth Metals. Acta Cystallographica 9:559-563.

[39] J.-W.Cut, F.E.Massoth, N.-Y.Topsøe.((1992) Studies of molybdena-alumina catalysts: XVIII. Lanthanum-Modified supports. Journal of Catalysis. 136: 361-377

[40] Y. Wu, M. Zarei-Chaleshton, B. Torres, T. Akter, C. Diaz-Moreno, G. B. Saupe, J. A. Lopez, R. R. Chianelli, D. Villagran (2017) Electrocatalytic hydrogen gas generation by cobalt molybdenum disulfide (CoMoS2) synthesized using alkyl-containing thiomolybdate precursors. International Journal of Hydrogen Energy 42:20669-20676.

[41] X. Hou, Y. Li, L. Cheng, X. Feng, H. Zhang, S. Han (2019) Cobalt-molybdenum disulfide supported on nitrogen-doped graphene towards an efficient hydrogen evolution reaction. International journal of hydrogen energy 44:11664-11674.

[42] A. Fonseca Lucredio, G. Jerkiewickz, E. Moreira Assaf (2007) Nickel catalysts promoted with cerium and lanthanum to reduce carbon formation in partial oxidation of methane reactions. Applied Catalysis A General 333: 90-95.

[43] I. Alstrup, I Chorkendorff, R. Candia, B. S. Clausen, H Topsoe (1982) A combined X- Ray photoelctron and Mossbauer Emission spectroscopy study of the state of cobalt in sulfided, supported and unsupported Co-Mo Catalysts. Journal of Catalysis 77: 397-409.

[44] Xiaoya Ma, Wei Zhang, Yida Deng, Cheng Zhong, Wenbin Hu, Xiaopeng Han (2018) Phase and composition-controlled synthesis of cobalt sulfide hollow nanospheres for electrocatalytic water splitting. Nanoscale 10:4816-4824.

[45] Tianjiao Ma, Mingmei Zhang, Hong Liu, Ying Wang (2019) Three-dimensional sulfur-doped graphene supported cobalt-molybdenum bimetallic sulfides nanocrystal with highly interfacial storage capability for supercapacitor electrodes. Electrochimica Acta 322:134762.

[46] Aokui Sun, Lu Xie, Dezhi Wang, Zhuangzhi Wu (2018) Enhanced energy storage performance from Co-decorated MoS2 nanosheets as supercapacitor electrode materials. Ceramics International 44:13434–13438.

[47] Xiaoya Ma, Wei Zhang, Yida Deng, Cheng Zhong, Wenbin Hu, Xiaopeng Han. (2018) Phase and composition controlled synthesis of cobalt sulfide hollow nanospheres for electrocatalytic water splitting. Nanoscale. 10: 4816-4824

[48] Tingting Huang, Jundong Xu, Yu Fan. (2018) Effects of concentration and microstructure of active phases on the selective hydrodesulfurization performance of sulfided CoMo/Al2O3 catalysts. Applied Catalysis B: Environmental. 220: 42-56

[49] Xiaoping Dai, Kangli Du, Zhanzhao Li, Mengzhao Liu, Yangde Ma, Hui Sun, Xin Zhang, and Ying Yang. (2015) Co-Doped MoS2 Nanosheets with the Dominant CoMoS Phase Coated on Carbon as an Excellent Electrocatalyst for Hydrogen Evolution. ACS Appllied Materials Interfaces. 7: 27242–27253

[50] Hongjuan Wang, Zhongping Li, Guanghua Li ,Feng Peng, HaoYu. (2015) Co3S4/NCNTs: A catalyst for oxygen evolution reaction. Catalysis Today. 245: 74-78

[51] Wei Zhang, Xiaoya Ma, Cheng Zhong, Tianyi Ma, Yida Deng, Wenbin Hu, and Xiaopeng Han. (2018) Pyrite-Type CoS2 Nanoparticles Supported on Nitrogen-Doped Graphene for Enhanced Water Splitting. Front Chem. 6: 569

[52] D. Xiong, Q.Zhang, W. Li, J. Li, X. Fu, M. Fátima Cerqueira, P. Alpuim and L. Liu (2017) Atomic-layer-deposited ultrafine MoS2 nanocrystals on cobalt foam for efficient and stable electrochemical oxygen evolution. Nanoscale 9:2711-2717.

[53] H.W. Wang , P. Skeldon, G.E. Thompson (1997) XPS studies of MoS2 formation from ammonium tetrathiomolybdate solutions. Surface and Coatings Technology 91:200-207.

[54] Minglin Xiang, Debao Li, Juan Zou, Wenhuai Li, Yuhan Sun, Xichun She (2010) XPS study of potassium-promoted molybdenum carbides for mixed alcohols synthesis via CO hydrogenation. Journal of Natural Gas Chemistry 19:151-155.

[55] X. Wu, X. Ding, W. Qin, W. He, Z. Jiang (2006) Enhanced photo-catalytic activity of TiO2 films with doped La prepared by micro-plasma oxidation method. Journal of Hazardous Materials 137:192-197.

[56] S. Anandan, A. Vinu, K.L.P. Sheeja Lovely, N. Gokulakrishnan, P. Srinivasu, T. Mori, V. Murugesan, V. Sivamurugan, and K Ariga (2007) Photocatalytic activity of La-doped ZnO for the degradation of monocrotophos in aqueous suspension 266:149-157.

[57] Liming Jin, Gaoran Li, Binhong Liu, Zhoupeng Li, Junsheng Zheng, Jim P. Zheng (2017) A novel strategy for high-stability lithium sulfur batteries by in situ formation of polysulfide adsorptive-blocking layer. Journal of Power Sources 355:147-153.

[58] Kaibin Tang, Changhua An, Pingbo Xie, Guozhen Shen, Yitai Qian (2002) Low-temperature synthesis and characterization of β-La2S3 nanorods. Journal of Crystal Growth 245: 304–308.

[59] Peisen Li, Wanqi Jie, and Huanyong Li (2011) Influences of Hot-Pressing Conditions on the Optical Properties of Lanthanum Sulfide Ceramics. J. Am. Ceram. Soc. 94:1162–1166.

[60] Lu Tian, Ti Ouyang, Kian Ping Loh, Jagadese J. Vittal. La2S3 thin films from metal organic chemical vapor deposition of single-source precursor. J. Mater. Chem. 16:272-277.

[61] I. Alstrup, I Chorkendorff, R. Candia, B. S. Clausen, H Topsoe (1982) A combined X- Ray photoelctron and Mossbauer Emission spectroscopy study of the state of cobalt in sulfided, supported and unsupported Co-Mo Catalysts. Journal of Catalysis 77: 397-409.

[62] K. Inamura, R. Prins (1994) The role of Co in unsupported Co-Mo sulfides in the hydrodesulfurization of thiophene. Journal of Catalysis 147:515-524.

[63] José Escobar, María C. Barrera,Jaime S. Valente,Dora A. Solís-Casados,Víctor Santes ,José E. Terrazas, and Benoit A.R. Fouconnier (2019). Dibenzothiophene Hydrodesulfurization over P-CoMo on Sol-Gel Alumina Modified by La Addition. Effect of Rare-Earth Content. Catalysts 9: 359; https://doi.org/10.3390/catal9040359

[64] A. Olivas, D.H. Galvan, G. Alonso, S. Fuentes (2009) Trimetallic NiMoW unsupported catalysts for HDS. Applied Catalysis A: General 352:10–16.

[65] Juan Manuel Quintana-Melgoza, Gabriel Alonso-Nunez, Donald Homero-Galvan, Miguel Avalos-Borja (2012) Comparative Activity of Ni-W and Co-Mo Sulfides Using Transition Metal Oxides as Precursors in HDS Reactions of DBT. Catalysis Letters 142:1082-1088.

[66] A. Olivas, G. Alonso, S. Fuentes (2006) The catalytic activity of Ni/W bimetallic sulfide nanostructured catalysts in the hydrodesulfurization of dibenzothiophene. Topics in Catalysis 39:175-179.

[67] P.A. Nikulshin, A.V. Mozhaev, K.I. Maslakov, A.A. Pimerzin, V.M. Kogan (2014) Genesis of HDT catalysts prepared with the use of Co2Mo10HPA and cobal citrate: Study of their gas and liquid sulfidation. Applied Catalysis B: Environmental 158-159:161-174.

[68] L. Alvarez, J. Espino, C. Ornelas, J.L. Rico, M.T. Cortez, G. Berhault, G. Alonso (2004) Comparative study of MoS2 and Co/MoS2 catalysts prepared by ex situ/in situ activation of ammonium and tetraalkylammonium thiomolybdates. Journal of Molecular Catalysis A: Chemical 210:105-117

.

Table 1: Operating parameters for the GC-MS and GC-FID, determination of DBT concentration

Parameter	GC-MS Setting	GC-FID Setting
Initial Oven Temperature	60 °C	100 °C
Final Oven Temperature	260 °C	250 °C
Injector Temperature	260 °C	250 °C
Ramp	20 °C/min	20 °C/min
Source Temperature	300 °C	
Gas Flow	He 2.0 mL/min	Air 450mL and 45mL H_2
Column	Perkin Elmer Elite-5	Perkin Elmer Elite-5
Injection volume	1.0 µL	1.0 µL

Table 2: LeBail fitting of ATM precursor.

Phase	Space Group	a (Å)	b (Å)	c (Å)	α°	β°	γ°	χ^2
ATM	PNMA	9.5551	6.9462	12.211	90	90	90	2.54

Table 3: LeBail fittings of fresh catalysts decomposed under a solvothermal decomposition in decahydronaphthalene solvent.

	Phase	Space Group	a (Å)	b (Å)	c (Å)	α°	β°	γ°	χ2
$CoMoS_2$	MoS_2	P63/MMC	3.1496	3.1496	12.3315	90	90	120	0.170
	Co_9S_8	FM3M	9.9246	9.9246	9.9246	90	90	90	
$La_{0.05}Co_{0.95}MoS_2$	MoS_2	P63/MMC	3.1321	3.1321	12.3584	90	90	120	0.379
	Co_9S_8	FM3M	9.9145	9.9145	9.9145	90	90	90	
$La_{0.10}Co_{0.90}MoS_2$	MoS_2	P63/MMC	3.1321	3.1321	12.3584	90	90	120	0.244
	Co_9S_8	FM3M	9.9145	9.9145	9.9145	90	90	90	
$La_{0.25}Co_{0.75}MoS_2$	MoS_2	P63/MMC	3.1318	3.1318	12.3265	90	90	120	0.267
	Co_9S_8	FM3M	9.9065	9.9065	9.9065	90	90	90	
	La_2S_3	PNMA	7.7454	4.1523	15.7205	90	90	90	

Table 4: LeBail fittings of used catalysts decomposed under a solvothermal decomposition in decahydronaphthalene solvent.

	Phase	Space Group	a (Å)	b (Å)	c (Å)	α°	β°	γ°	χ2
$CoMoS_2$	MoS_2	P63/MMC	3.1496	3.1496	12.3315	90	90	120	0.208
	Co_9S_8	FM3M	9.9246	9.9246	9.9246	90	90	90	
$La_{0.05}Co_{0.95}MoS_2$	MoS_2	P63/MMC	3.1320	3.1320	12.3584	90	90	120	0.183
	Co_9S_8	FM3M	9.9145	9.9145	9.9145	90	90	90	
$La_{0.10}Co_{0.90}MoS_2$	MoS_2	P63/MMC	3.1259	3.1259	12.2775	90	90	120	0.469
	Co_9S_8	FM3M	9.9478	9.9478	9.9478	90	90	90	
$La_{0.25}Co_{0.75}MoS_2$	MoS_2	P63/MMC	3.1382	3.1082	12.3898	90	90	120	0.318
	Co_9S_8	FM3M	9.8472	9.8472	9.8472	90	90	90	
	La_2S_3	PNMA	7.7963	4.1560	15.8667	90	90	90	

Table 5: Surface aera of the $CoMoS_2$ and $La_{0.X}Co_{1-0.X}Mos_2$ catalysts

Sample	S_{BET} $(m^2/g)^a$
$CoMoS_2$	71.60
$La_{0.05}Co_{0.95}MoS_2$	96.19
$La_{0.10}Co_{0.9}MoS_2$	66.63
$La_{0.25}Co_{0.75}MoS_2$	60.91

Table 6: Mass percent of Mo, S, Co and La and mole fraction found in the $CoMoS_2$ and $La_{0.X}Co_{1-0.X}MoS_2$ catalysts determined from EDS analysis.

Sample	Mo%	Mo (mole)	S%	S (mole)	Co%	Co (mole)	La%	La (mole)	La:Co
As Synthesized									
$CoMoS_2$	42.61	0.444	31.72	0.990	25.66	0.435			
$La_{0.05}Co_{0.95}MoS_2$	40.96	0.426	32.04	0.999	24.01	0.407	2.99	0.0215	0.053
$La_{0.10}Co_{0.90}MoS_2$	41.19	0.429	30.79	0.960	24.79	0.420	3.25	0.0234	0.056
$La_{0.25}Co_{0.75}MoS_2$	43.39	0.452	31.20	0.973	19.91	0.338	5.51	0.0397	0.117
After one Cycle									
$CoMoS_2$	39.75	0.414	30.30	0.945	29.95	0.508			
$La_{0.05}Co_{0.95}MoS_2$	33.84	0.353	26.57	0.829	37.92	0.642	1.66	0.0120	0.019
$La_{0.10}Co_{0.90}MoS_2$	42.07	0.439	30.21	0.942	20.38	0.421	2.85	0.0206	0.049
$La_{0.25}Co_{0.75}MoS_2$	42.6	0.444	31.27	0.975	22.90	0.355	5.17	0.0373	0.105

Table 7: Ratio of C 1s peak areas extracted from XPS spectra of fresh and used catalysts.

Sample	Carbon peak area	Ratio (After:Before)
$CoMoS_2$ Fresh	79293	1.366
$CoMoS_2$ Used	108306	
$La_{0.05}Co_{0.95}MoS_2$ Fresh	78960	1.201
$La_{0.05}Co_{0.95}MoS_2$ Used	94792	
$La_{0.10}Co_{0.90}MoS_2$ Fresh	62110	1.000
$La_{0.10}Co_{0.90}MoS_2$Usedt	62108	
$La_{0.25}Co_{0.75}MoS_2$ Fresh	97001	
$La_{0.25}Co_{0.75}MoS_2$ Used	94234	0.97

Table 8: Catalytic activities calculated for the synthesized $CoMoS_2$, $La_{0.05}Co_{0.95}MoS_2$, $La_{0.10}Co_{0.90}MoS_2$, and the $La_{0.25}Co_{0.75}MoS_2$ with literature values for other HDS catalysts. lanthanum substituted

Catalyst	K ($x10^{-7}$ mol $s^{-1}g^{-1}$)	Literature K ($x10^{-7}$ mol $s^{-1}g^{-1}$)
$CoMoS_2$	6.80	24.5, 9.27 [5], 3.07[63]
$NiMoS_2$	N/A	4.61[63]
MoS_2	N/A	2.74[63]
$NiMoS_2$	N/A	7.2[62]
$NiMoS_2$	N/A	11[62,64]
$La_{0.05}Co_{0.95}MoS_2$	6.51	Present study
$La_{0.10}Co_{0.90}MoS_2$	10.7	Present study
$La_{0.25}Co_{0.75}MoS_2$	10.7	Present study

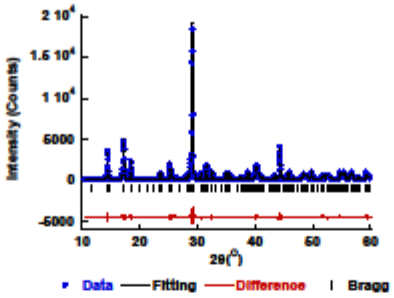

Figure 1

Figure 1: Powder XRD pattern of the synthesized ammonium tetrathiomolybdate and fitting, difference between the data and the fitting, and Bragg peaks.

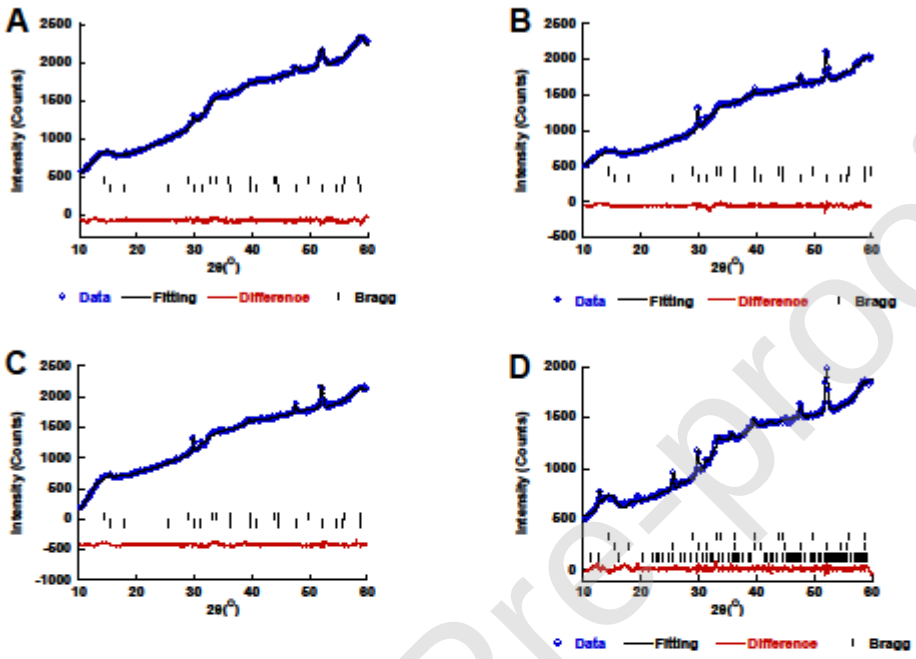

Figure 2

Figure 2: A. Powder XRD patterns of fresh $CoMoS_2$, **B.** $La_{0.05}Co_{0.95}MoS_2$, **C.** $La_{0.10}Co_{0.90}MoS_2$

and **D.** $La_{0.25}Co_{0.75}MoS_2$ synthesized using solvothermal decomposition with decahydronaphthalene solvent.

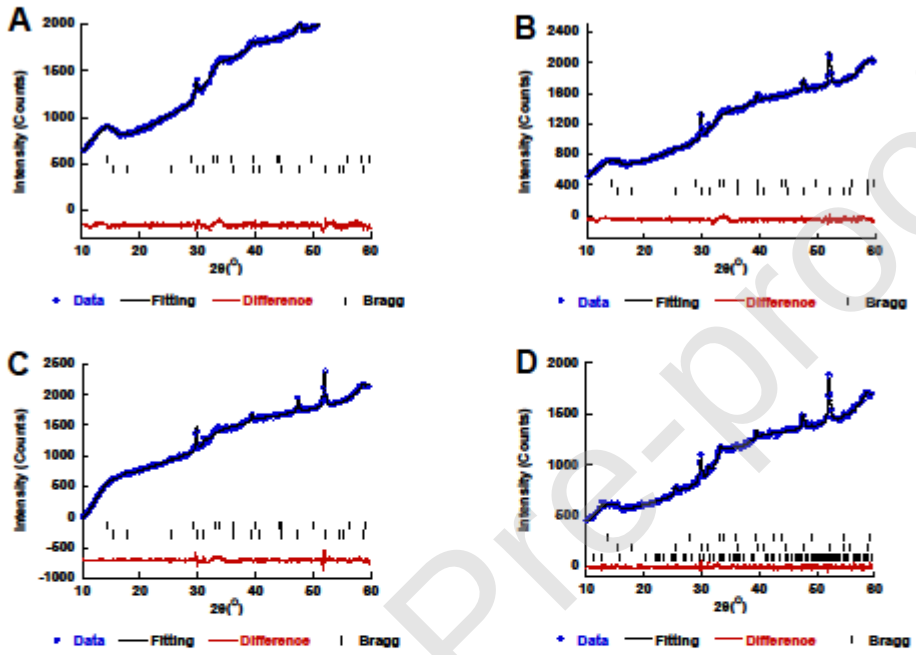

Figure 3

Figure 3: A. Powder XRD patterns of used $CoMoS_2$, **B.** $La_{0.05}Co_{0.95}MoS_2$, **C.** $La_{0.10}Co_{0.90}MoS_2$ and **D.** $La_{0.25}Co_{0.75}MoS_2$ synthesized using solvothermal decomposition with decahydronaphthalene solvent.

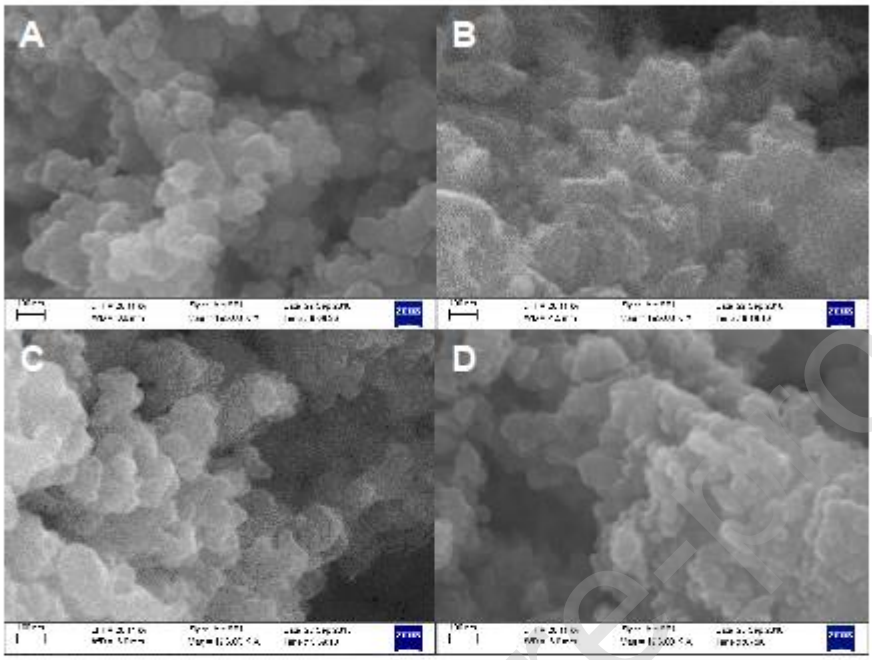

Figure 4

Figure 4 A. SEM images of fresh $CoMoS_2$, **B.** $La_{0.05}Co_{0.95}MoS_2$, **C.** $La_{0.10}Co_{0.90}MoS_2$, and **D.** $La_{0.25}Co_{0.75}MoS_2$ decomposed under a solvothermal decomposition in decahydronaphthalene solvent.

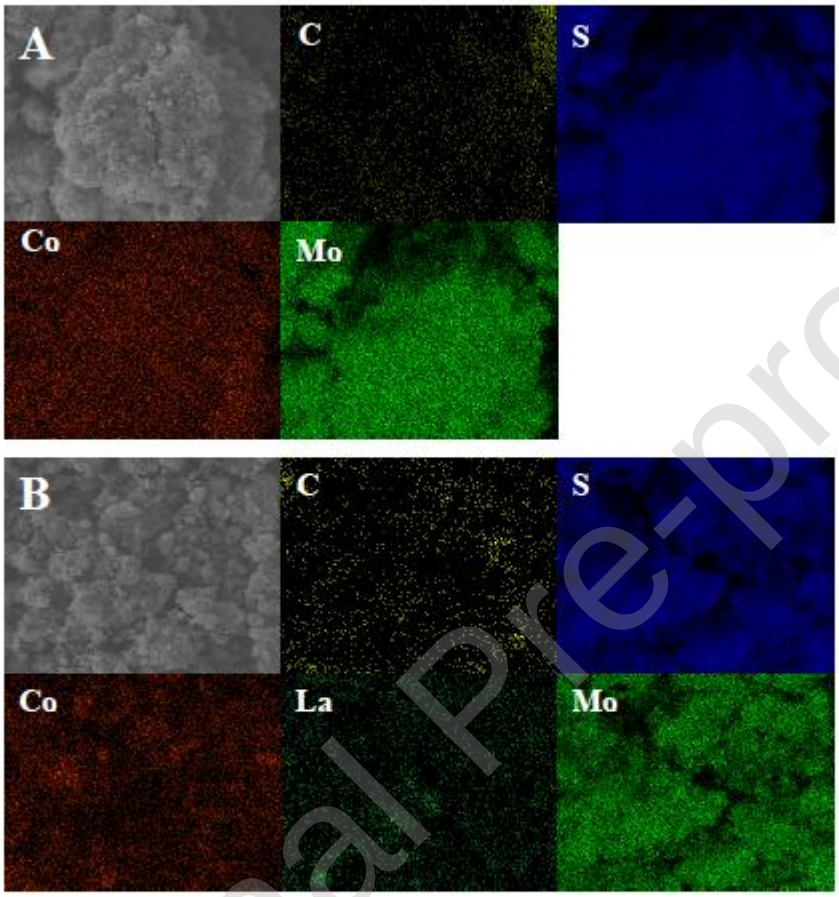

Figure 5

Figure 5: A. EDS map of fresh $CoMoS_2$ catalyst decomposed under a solvothermal decomposition in decahydronaphthalene solvent showing carbon, cobalt, molybdenum and sulfur. **B.** EDS map of

fresh $La_{0.25}Co_{0.75}MoS_2$ catalyst decomposed under a solvothermal decomposition in decahydronaphthalene solvent showing carbon, cobalt, lanthanum, molybdenum and sulfur.

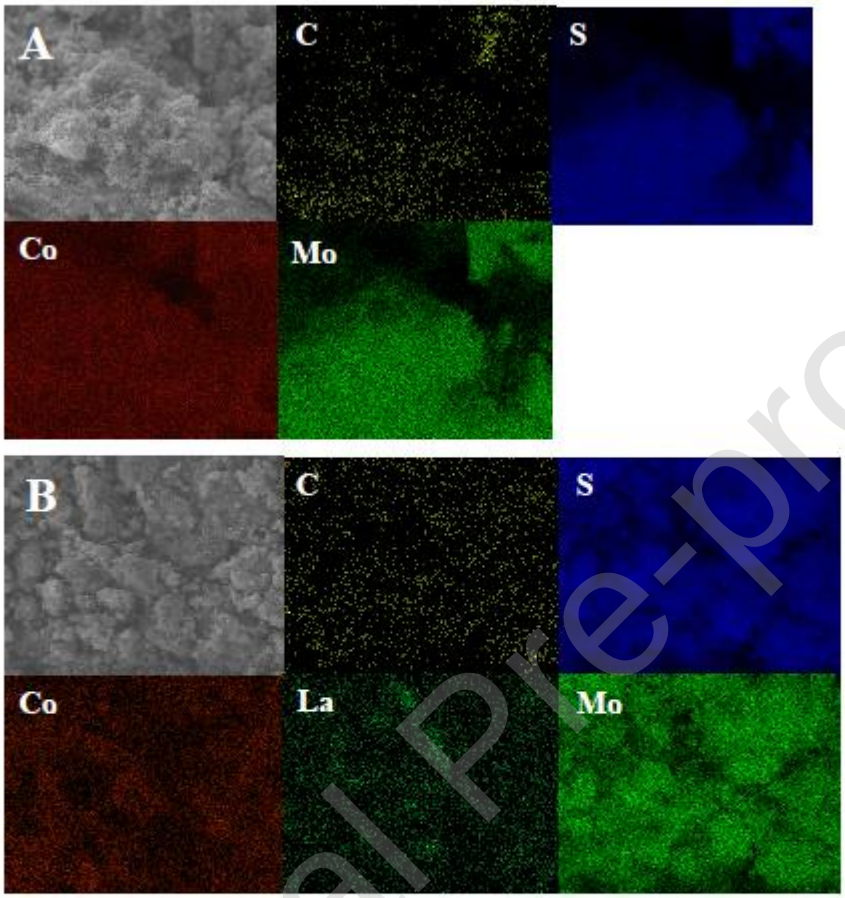

Figure 6

Figure 6 A: EDS map of used $CoMoS_2$ catalyst decomposed under a solvothermal decomposition in decahydronaphthalene solvent showing carbon, cobalt, molybdenum and sulfur. **B.** EDS map

of used $La_{0.25}Co_{0.75}MoS_2$ catalyst decomposed under a solvothermal decomposition in decahydronaphthalene solvent showing carbon, cobalt, lanthanum, molybdenum and sulfur.

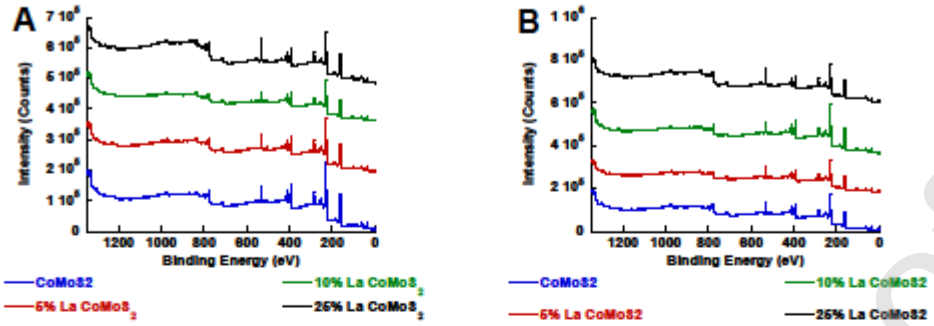

Figure 7

Figure 7: A. XPS spectra of fresh catalysts decomposed under a solvothermal decomposition in decahydronaphthalene solvent. **B.** XPS spectra of spent catalysts decomposed under a solvothermal decomposition in decahydronaphthalene solvent.

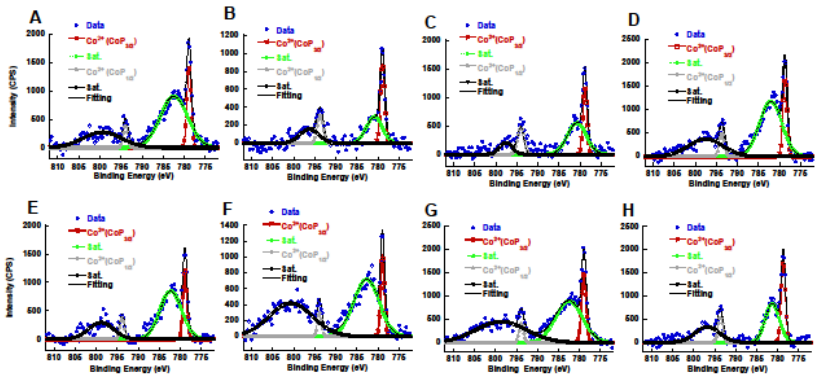

Figure 8

Figure 8: Co2P XPS spectra of $CoMoS_2$ as prepared (**A**), $La_{0.05}Co_{0.95}MoS_2$ as prepared (**B**), $La_{0.10}Co_{0.90}MoS_2$ as prepared (**C**), $La_{0.25}Co_{0.75}MoS_2$ as prepared (**D**) $CoMoS_2$ after one catalytic cycle (**E**), $La_{0.05}Co_{0.95}MoS_2$ after one catalytic cycle (**F**), $La_{0.10}Co_{0.90}MoS_2$ after one catalytic cycle (**G**), and $La_{0.25}Co_{0.75}MoS_2$ after one catalytic cycle (**H**).

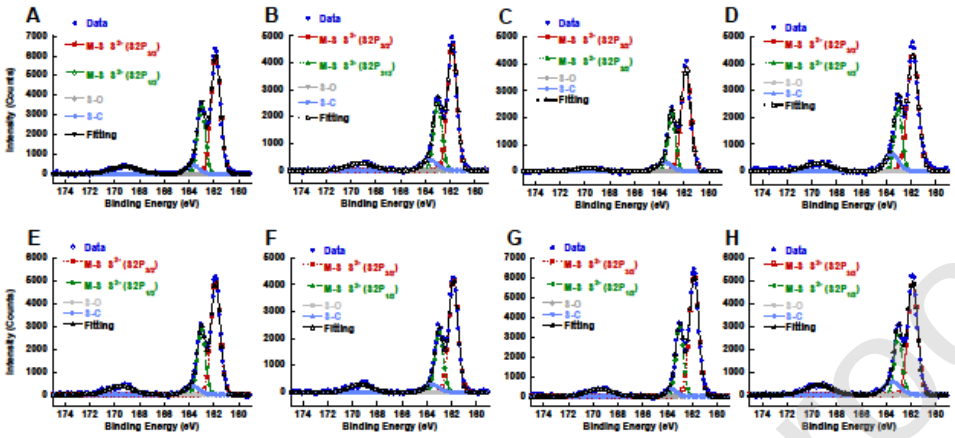

Figure 9

Figure 9: S2P XPS spectra of $CoMoS_2$ as prepared (**A**), $La_{0.05}Co_{0.95}MoS_2$ as prepared (**B**), $La_{0.10}Co_{0.90}MoS_2$ as prepared (**C**), $La_{0.25}Co_{0.75}MoS_2$ as prepared (**D**) $CoMoS_2$ after one catalytic cycle (**E**), $La_{0.05}Co_{0.95}MoS_2$ after one catalytic cycle (**F**), $La_{0.10}Co_{0.90}MoS_2$ after one catalytic cycle (**G**), and $La_{0.25}Co_{0.75}MoS_2$ after one catalytic cycle (**H**)

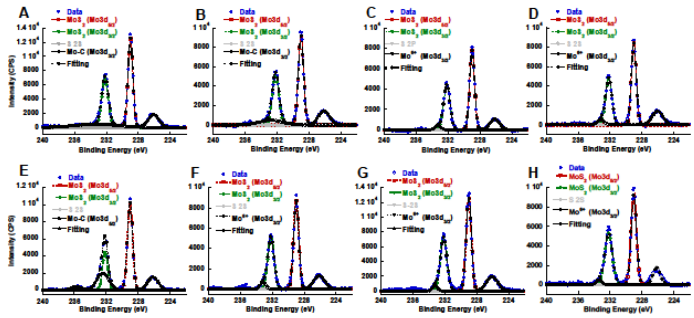

Figure 10

Figure 10: Mo3d XPS spectra of $CoMoS_2$ as prepared (**A**), $La_{0.05}Co_{0.95}MoS_2$ as prepared (**B**), $La_{0.10}Co_{0.90}MoS_2$ as prepared (**C**), $La_{0.25}Co_{0.75}MoS_2$ as prepared (**D**) $CoMoS_2$ after one catalytic cycle (**E**), $La_{0.05}Co_{0.95}MoS_2$ after one catalytic cycle (**F**), $La_{0.10}Co_{0.90}MoS_2$ after one catalytic cycle (**G**), and $La_{0.25}Co_{0.75}MoS_2$ after one catalytic cycle (**H**).

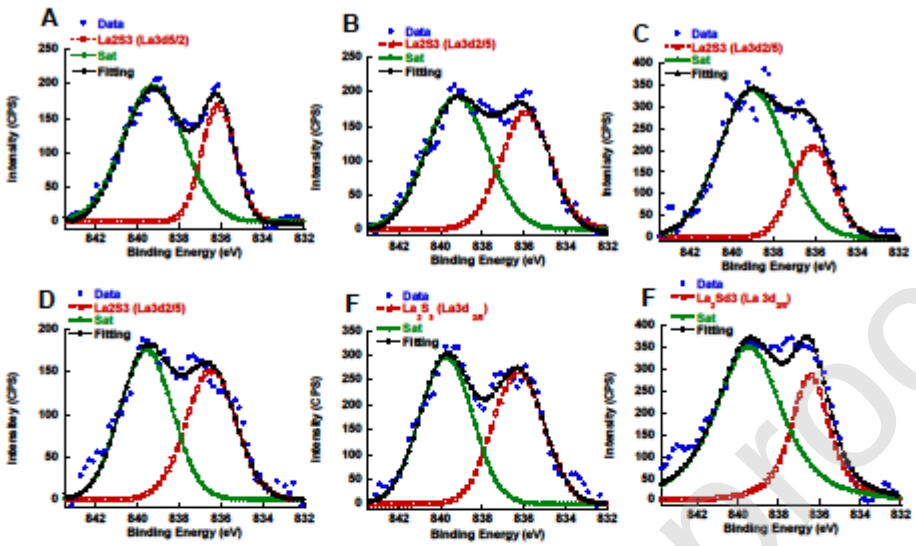

Figure 11: La3d$_{5/2}$ XPS spectra of $La_{0.05}Co_{0.95}MoS_2$ as prepared (**A**), $La_{0.10}Co_{0.90}MoS_2$ as prepared (**B**), $La_{0.25}Co_{0.75}MoS_2$ as prepared (**C**), $La_{0.05}Co_{0.95}MoS_2$ after one catalytic cycle (**D**), $La_{0.10}Co_{0.90}MoS_2$ after one catalytic cycle (**E**), and $La_{0.25}Co_{0.75}MoS_2$ after one catalytic cycle (**F**)

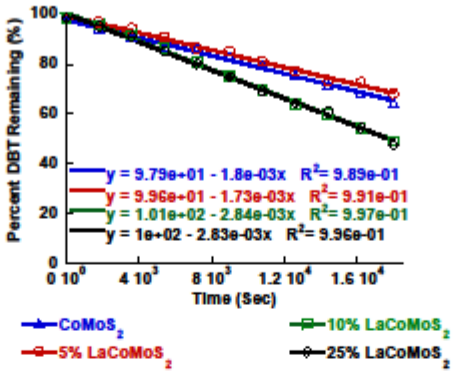

Figure 12

Figure 12: Results from catalytic testing of catalysts of $CoMoS_2$, $La_{0.05}Co_{0.95}MoS_2$, $La_{0.10}Co_{0.90}MoS_2$, and $La_{0.25}Co_{0.75}MoS_2$ catalysts at 350°C with 160 psi H_2 initial pressure.

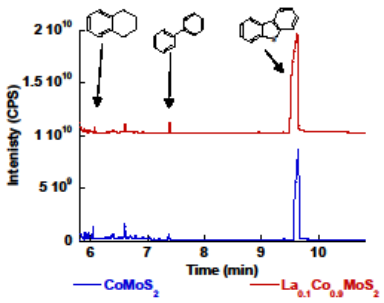

Figure 13

Figure 13: Chromatogram of the reaction at t=0, initially reached 350° for the $La_{0.10}Co_{0.90}MoS_2$(top) and the $CoMoS_2$ (bottom).

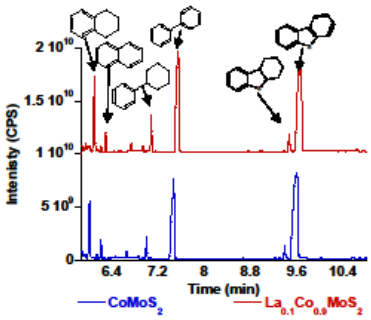

Figure 14

Figure 14: Chromatogram of the reaction after 300 minutes Reaction for the $La_{0.10}Co_{0.90}MoS_2$ (top) and $CoMoS_2$ (bottom) with DBT.